Research Article

Julian Schwab*, Florian Mangold, Bettina Frank, Timothy J. Davis and Harald Giessen

Skyrmion bag robustness in plasmonic bilayer and trilayer moiré superlattices

Abstract: Twistronics is studied intensively in twisted 2D heterostructures and its extension to trilayer moiré structures has proven beneficial for the tunability of unconventional correlated states and superconductivity in twisted trilayer graphene. Just recently, the concept of twistronics has been applied to plasmonic lattices with nontrivial topology, demonstrating that bilayer moiré skyrmion lattices harbor multi-skyrmion textures called skyrmion bags. Here, we explore the properties of plasmonic trilayer moiré superlattices that are created by the interference of three twisted skyrmion lattices. More specifically, we explore the properties of periodic superlattices and their topological invariants. We also demonstrate that twisted trilayer skyrmion lattices harbor the same skyrmion bags as twisted bilayer skyrmion lattices. We quantify the robustness of these skyrmion bags by the stability of their topological numbers against certain disturbance fields that leads to experimental designs for topological textures with maximum robustness.

Keywords: plasmonics; topology; topological robustness; skyrmion bags; plasmonic twistronics; moire superlattices

*Corresponding author: Julian Schwab, 4th Physics Institute, Research Center SCoPE, and Integrated Quantum Science and Technology Center, University of Stuttgart, 70569 Stuttgart, Germany,
E-mail: julian.schwab@pi4.uni-stuttgart.de.
https://orcid.org/0000-0003-3749-6145
Florian Mangold, **Bettina Frank and Harald Giessen**, 4th Physics Institute, Research Center SCoPE, and Integrated Quantum Science and Technology Center, University of Stuttgart, 70569 Stuttgart, Germany
Timothy J. Davis, 4th Physics Institute, Research Center SCoPE, and Integrated Quantum Science and Technology Center, University of Stuttgart, 70569 Stuttgart, Germany; Faculty of Physics and Center for Nanointegration, Duisburg-Essen (CENIDE), University of Duisburg-Essen, 47048 Duisburg, Germany; and School of Physics, University of Melbourne, Parkville, Victoria 3010, Australia. https://orcid.org/0000-0002-7299-4900

1 Introduction

Moiré patterns in atomic systems can be constructed by stacked layers of van der Waals materials with a relative twist and/or lattice mismatch. The moiré pattern modulates the lattice periodically resulting in a superlattice demonstrating a variety of strongly correlated phases. These superlattices were studied intensively in twisted bilayer graphene, where this enables superconductivity [1], correlated insulating states [2], and strange metal behavior [3]. Recently, huge attention has also been drawn towards trilayer moiré superlattices (TMSLs) such as twisted trilayer graphene [4]–[9], hexagonal boron nitride (h-BN)-graphene heterostructures [10]–[12], and transition metal dichalcogenide heterostructures [13]–[15]. The introduction of a third layer modulates the bilayer moiré superlattice and leads to long-range super-moiré patterns that are controlled by the twist angle of the third layer. This new twist angle adds more degrees of freedom and offers more flexibility, e.g., to tune unconventional correlated states and superconductivity in twisted trilayer graphene [4], [8], [9], [16].

In optics, twisted bilayer photonic lattices have been created using metasurfaces, metamaterials, and photonic crystals [17]–[23]. However, trilayer photonic lattices have so far only been realized to study the far field coupling of a moiré nano particle lattice laser [24] with many remaining aspects to be investigated. Here we focus on the topology of trilayer twisted optical lattices with nontrivial topological features such as skyrmions [25]. These are three-dimensional topological defects on a two-dimensional plane that were observed first in solid materials [26]–[29] and liquid crystals [30], [31]. Skyrmions were also demonstrated in optics [32]–[35] and particularly in plasmonic systems [36]–[38], where skyrmion lattices emerge through interference of surface plasmon polariton (SPP) waves. Recently, the concept of twistronics has been applied to such plasmonic lattices in order to create plasmonic moiré skyrmion superlattices [39]. By investigating their topology, it was demonstrated that they harbor skyrmion bags [28], [31], [40], which are multi-skyrmion textures that consist of N skyrmions contained within a skyrmion boundary of opposite winding

number -1. Their size is controllable by the twist angle and the center of rotation, and they feature a degree of robustness against deviations of the twist angle [39].

Here, we extend the concept of 'plasmonic twistronics' to trilayer plasmonic skyrmion superlattices, consisting of three twisted plasmonic skyrmion lattices. We present numerical results of commensurate super-moiré lattices with large periodicity and a super-cell with very large topological charge. We discover that they feature skyrmion bags of new shapes that are not possible to realize in twisted bilayer skyrmion lattices. In addition to these new bag textures, all skyrmion bags of the bilayer system can be recreated using mirror-symmetric trilayer skyrmion lattices. We demonstrated previously that bilayer skyrmion bags possess a degree of topological robustness against deviations of the twist angle [39]. This robustness increases for smaller skyrmion bags that appear at larger twist angles.

In the following, we present a method to quantify the topological robustness of skyrmion bags by testing their stability against perturbational fields. This allows us to compare the skyrmion bag robustness in bilayer and trilayer moiré superlattices and determine the ideal twist angles in these systems. Such a comparison of the topological stability is helpful when designing the ideal structures for experimental realizations. We demonstrate that this general approach can also be used to compare the robustness of different topological textures and assess their chance of a successful experimental implementation. Our results extend the toolbox of plasmonic twistronics and provide a valuable method to determine topological textures in wave systems with high topological stability. These textures might find subsequent application in structured light–matter interactions.

2 Plasmonic trilayer moiré skyrmion superlattices

Plasmonic lattices can be excited by specific coupling structures that are etched into a single crystalline gold flake using ion beam lithography [36], [41], [42]. A laser pulse incident on such grooves in a metal surface generates charge excitations on their edges, from where SPP waves are launched and propagate towards the center of the structure. The interference pattern of these plasmon waves can exhibit different topological features in their electric field vectors [36], [41] and their spin angular momentum vectors [37], [42]–[44] that are controlled by the shape of the coupling structure and the resulting propagation direction and phase

shift of the SPPs [45]. In the case of a hexagonal coupling structure, a plasmonic skyrmion lattice can be generated [36]. Plasmonic skyrmion lattices exhibit a six-fold symmetry [42], reminiscent of two-dimensional honeycomb lattices in graphene, h-BN, or hexagonal TMDC monolayers. Moiré lattices have been investigated intensively using these van-der-Waals materials, and recent research has also been directed towards twisted trilayer heterostructures, such as twisted trilayer graphene.

Using such materials, TMSLs are created by stacking three layers of a 2D lattice with a relative twist, as illustrated in Figure 1a. Superimposing, the three layers results in a super-moiré lattice as illustrated at the bottom. The moiré twist angles ϕ_{12} (ϕ_{23}) between the consecutive lattices L1 and L2 (L2 and L3) are connected to the twist between L1 and L3 by $\phi_{13} = \phi_{12} + \phi_{23}$.

In optics, and specifically in plasmonics, moiré lattices are created by the interference of superimposed photonic lattices with a relative twist. Here, we focus on plasmonic trilayer moiré skyrmion lattices that are created by the interference of three twisted skyrmion lattices. The corresponding coupling structure is composed of three twisted hexagons, with each hexagon contributing a skyrmion lattice with different orientation. The three hexagons are combined into a coupling structure which consists of 18 line
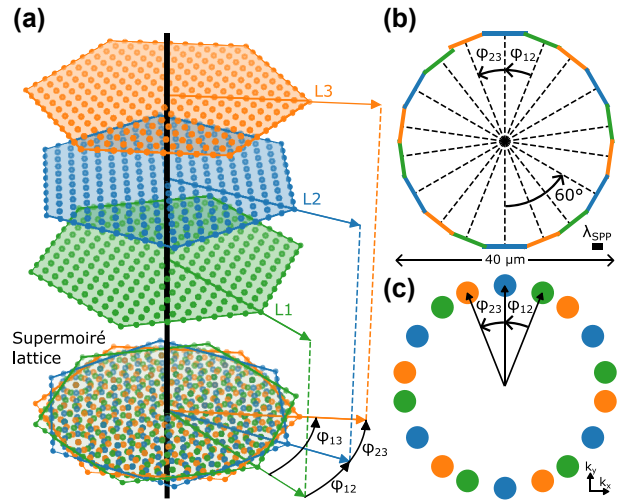

Figure 1: Plasmonic super-moiré skyrmion lattices. (a) Super-moiré lattice created by three hexagonal lattices with relative twist ϕ_{12} between the first and second lattice (L1 and L2) and ϕ_{23} between the second and third lattice (L2 and L3). In plasmonics, the lattices are superimposed in a single layer as illustrated at the bottom. (b) Corresponding coupling structure of a super-moiré skyrmion lattice. The coupling structure consists of three tilted hexagons, generating three skyrmion lattices with relative twists. (c) Schematic Fourier decomposition of a moiré skyrmion superlattice, where the colors originate from the boundaries in (b) and the lattice colors in (a).

segments. The coupling structure is illustrated in Figure 1b, where the three colors of the boundaries illustrate the origin of the boundaries from the three hexagons. The excitation of SPPs from all boundaries with the same efficiency is realized by using circularly polarized light. This creates a phase shift between SPPs that are launched from boundaries with different orientation, as a result of spin–orbit coupling [45]. To regain constructive interference in the center of the structure, this phase shift is compensated by adjusting the positions of the boundaries akin to an Archimedean spiral. The Fourier decomposition of the resulting skyrmion TMSL electric field distribution in Figure 1c highlights the six-fold symmetry of the three skyrmion lattices and their hexagonal excitation boundaries, as well as the moiré twist angles between them.

Bilayer moiré superlattices possess long-range aperiodic order and are hence quasicrystalline [9], [46] for general twist angles. Nonetheless, periodic bilayer structures can be obtained using specific twist angles that rotate a lattice site of one layer onto a lattice site of the other layer. The corresponding commensurability in six-fold symmetry has been first derived for twisted bilayer graphene [47],

[48] and can be denoted by the integers m and n with the corresponding mapping

$$m\boldsymbol{a}_1 + n\boldsymbol{a}_2 \rightarrow n\boldsymbol{a}_1 + m\boldsymbol{a}_2, \quad m, n \in \mathbb{Z}, \qquad (1)$$

as illustrated in Figure 2a and b. These angles have recently also been utilized to create periodic plasmonic bilayer moiré skyrmion superlattices [39]. In the case of three layers, the moiré pattern is defined by setting two out of the three twist angles $\{\phi_{12}, \phi_{23}, \phi_{13}\}$. This effectively creates two bilayer moiré patterns that are combined to a more complex super-moiré pattern. Periodicity of the TMSL is achieved by choosing both individual twist angles to be bilayer commensurate angles that fulfill the moiré mapping equation (1) [5], [49], [50]. With this approach, a family of super-moiré skyrmion lattices are generated and depicted in Figure 2c–g with their associated superlattice vectors. Mathematical details about the commensurability and the resulting superlattice period are included in the supplement. The electric field distributions are derived assuming infinitely long boundary lines enabling the approximation of the SPP wave as a plane wave. This approximation results in an infinitely large field of view allowing the periodicity to be clearly
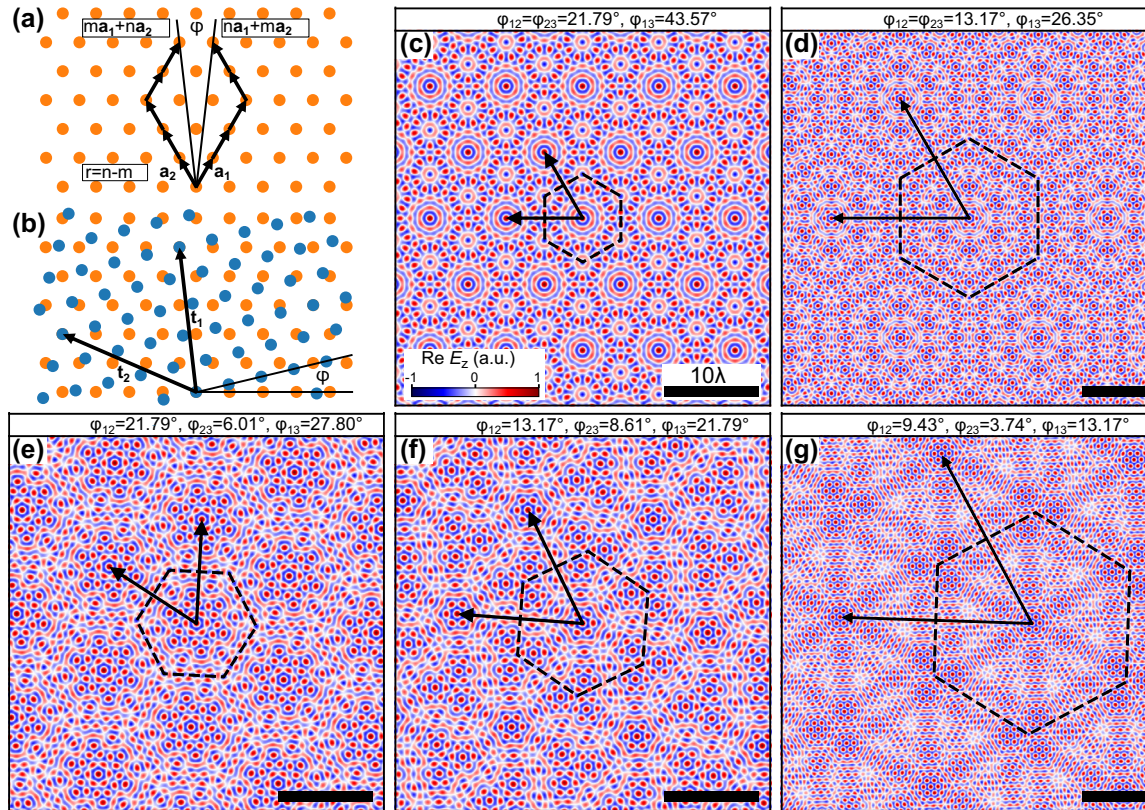

Figure 2: Periodic plasmonic super-moiré skyrmion lattices. (a) Periodic bilayer superlattices are created by mapping the lattice site $n\boldsymbol{a}_1 + m\boldsymbol{a}_2$ to $m\boldsymbol{a}_1 + n\boldsymbol{a}_2$ using the twist angle ϕ. (b) Moiré superlattice and superlattice vectors $\boldsymbol{t}_1$ and $\boldsymbol{t}_2$ for the rotation ϕ indicated in (a). In the case of three twisted lattices commensurability is achieved if the twist angles ϕ_{12} and ϕ_{13} are both such bilayer commensurate angles. (c–g) Exemplary periodic trilayer moiré skyrmion superlattices and their superlattice vectors. The superlattice unit cells are surrounded by dashed lines.

observed. In practice, the field of view is limited by the size of the structure and the duration of the excitation pulse.

3 Topological properties of trilayer moiré skyrmion superlattices

We analyze the local topology of the TMSL vector fields using the skyrmion number density

$$s = \frac{1}{4\pi}\hat{\boldsymbol{e}} \cdot \left(\frac{\partial \hat{\boldsymbol{e}}}{\partial x} \times \frac{\partial \hat{\boldsymbol{e}}}{\partial y} \right), \tag{2}$$

where $\hat{\boldsymbol{e}} = \boldsymbol{E}(r,t)/\|\boldsymbol{E}(r,t)\|$ is the unit vector of the SPP electric field. The skyrmion number or topological charge is defined as $S = \int_{\sigma} s\, dA$, where σ is the local region in which the topology is examined. In skyrmion lattices each unit cell consists of a skyrmion with $S = 1$. Analogously, the superlattice unit cells of bilayer [39] and trilayer skyrmion moiré superlattices possess a well-defined topological charge that can become very large for large periodicities of the superlattice. These topological charges are rigorously defined by the moiré superlattice and can therefore be used to characterize its topology. All topological charges of the super unit cells of Figure 2 are listed in Table 1. These values differ from the total number of skyrmion lattice sites that are contained in the super unit cell. This is because the twisted skyrmion lattices are superimposed in a single plane, which leads to an interference of these lattices. The interference can merge multiple skyrmions of different lattices to single elongated skyrmions. This decreases the total topological charge and gives rise to new topological features in the moiré superlattice such as skyrmion bags. Skyrmion bags have been identified first in liquid crystals and chiral magnets [28], [31],

Table 1: Calculated skyrmion numbers in super unit cells of trilayer moiré superlattices. The commensurate twist angles ϕ_{12}, ϕ_{13} and ϕ_{23} are denoted using the coprime integers m and r as explained in the main text. Counting the number of skyrmions of the individual lattices that are contained in the super unit cell yields $S_{\text{individual layers}}$. However, in the moiré superlattice the three lattices are superimposed within a single layer, which leads to an interference of the lattices. The resulting overlap of skyrmions decreases the observed skyrmion number of the superlattice unit cell to $S_{\text{unit cell}}$.

ϕ_{12} (°)	ϕ_{13} (°)	ϕ_{23} (°)	$S_{\text{individual layers}}$	$S_{\text{unit cell}}$
21.79 (1, 1)	43.57	21.79 (1, 1)	49	25
13.17 (2, 1)	26.35	13.17 (2, 1)	361	139
21.79 (1, 1)	26.80 (2, 3)	6.01	91	31
13.17 (2, 1)	21.79 (1, 1)	8.61	133	61
9.43 (3, 1)	13.17 (2, 1)	3.74	703	211

[40] and have recently been discovered in plasmonic twisted bilayer skyrmion lattices. They represent multi-skyrmion configurations, where N skyrmions with $S = 1$ are enclosed within a larger skyrmion. This surrounding skyrmion has oppositely oriented field components and therefore $S = -1$. Consequently, the total topological charge of a skyrmion bag is $S_{\text{bag}} = N - 1$.

In moiré skyrmion lattices, skyrmion bags are created through the interference of overlapping skyrmions. This interference creates a closed loop with positive out-of-plane field component. The size of the loop is dependent on the twist angle and the rotation center and encloses a cluster of N individual skyrmions, thus forming the skyrmion bag. Likewise, the cluster skyrmions are also composed of multiple overlapping skyrmions. However, their displacement is typically not large enough for them to merge with neighboring skyrmions which is why they form elongated skyrmions. The skyrmion number of the cluster can be obtained by integrating the skyrmion number density using an integration boundary that is set along the edge of the non-rotated unit cells (red dashed line of Figure 3e). For the full skyrmion bag the integration boundary can be set along the positions of the surrounding overlapping skyrmions (black dashed line of Figure 3e).

These skyrmion bags can be observed in and around the center of the superlattice unit cells of Figure 2. Additionally, trilayer moiré lattices give rise to skyrmion bag textures which contain other skyrmion bags (see Figure 2e–g) and therefore have new topological charges that may not be possible to achieve in the bilayer system.

All skyrmion bags of the twisted bilayer skyrmion lattices can also be realized in the trilayer system using a mirror-symmetric structure with $\phi_{12} = \phi_{23}$. With such an approach, the smallest skyrmion bags are numerically calculated and depicted in Figure 3. As in the bilayer system, a change of the center of rotation is related to a changed symmetry of the super-moiré pattern and can be used to realize skyrmion bags of additional sizes. The three different rotation centers P_1, P_2, and P_3 are marked in Figure 3a–c.

4 Robustness of skyrmion bags in twisted bilayer and trilayer skyrmion lattices

The skyrmion bags of Figure 3 are generated by the interference of three skyrmion lattices instead of two as in Ref. [39]. This is illustrated by the markers in Figure 3e that indicate the positions of the skyrmions of the individual lattices. It
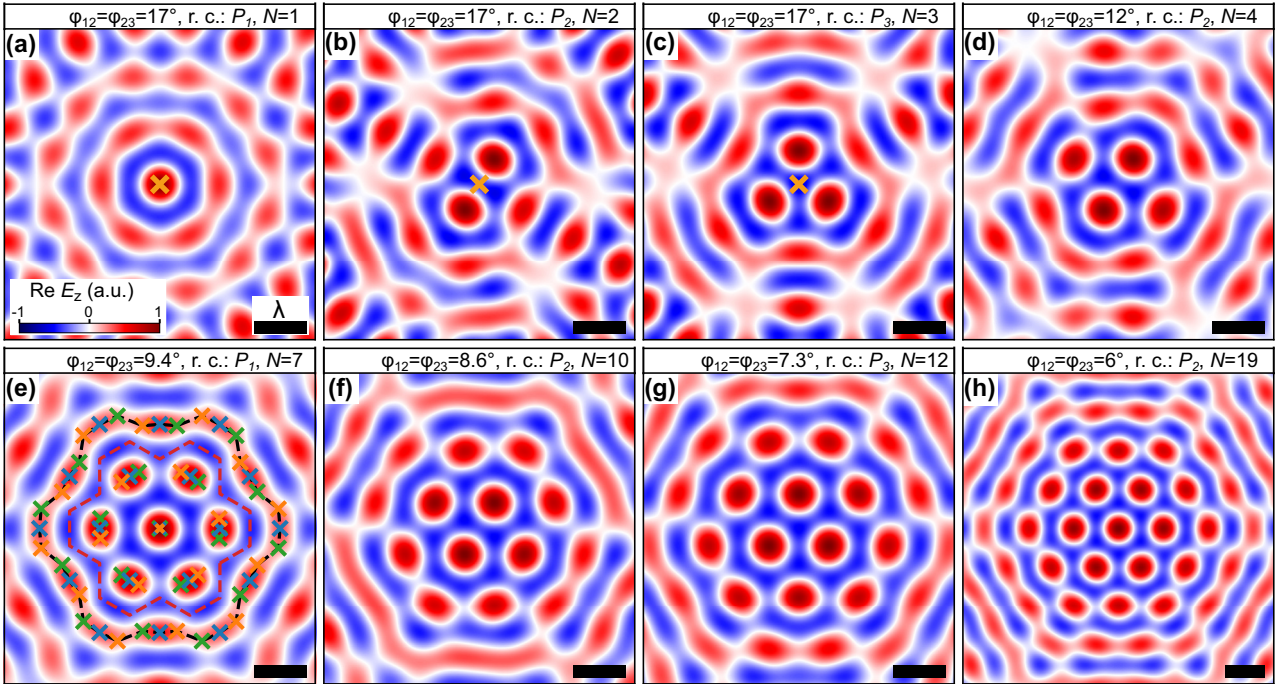
Figure 3: Skyrmion bags in super-moiré skyrmion lattices comprising (a) 1, (b) 2, (c) 3, (d) 4, (e) 7, (f) 10, (g) 12 and (h) 19 skyrmions. Skyrmion bags in twisted trilayer skyrmion lattices with mirror-symmetric twist angles $\phi_{12} = \phi_{23}$. The size of the skyrmion bags is controlled by these twist angles and the rotation centers (r. c.). The three rotation centers P_1, P_2 and P_3 are indicated by the orange markers in (a), (b), and (c), respectively. In (e), the position of the skyrmions of the three skyrmion lattices are indicated by the markers and the integration boundary of the skyrmion bag (the cluster within the bag) is indicated by the black (red) dashed line.

can be recognized that the skyrmions of the cluster within the bag are created by three instead of two overlapping skyrmions that form a more elongated single skyrmion. Additionally, the surrounding bag skyrmion with $S = -1$, is created by the interference of $3/2$ times more skyrmions and is therefore more homogeneous than in twisted bilayer skyrmion lattices. In the following, we illustrate that this increased overlap improves the stability of some skyrmion bags, enabling the choice of the ideal coupling structure to achieve a certain topological texture with maximum robustness.

We quantify the robustness of a topological texture by its ability to preserve its topological numbers when a disturbance field is applied. Here, the disturbance field consists of 50 SPP plane waves with randomly distributed amplitude, phase, propagation constant, and propagation direction (see Supplementary for details). It is important to note that the propagation constants are chosen to be normally distributed around the propagation constant of the initial field with only a small standard deviation. This is because perturbating waves with other propagation constants could be easily removed via Fourier filtering. Using a perturbation of this kind, the total field in the structure is given by

$E = E_0 + g \frac{\text{Mean}(\|E_0\|)}{\text{Mean}(\|E_V\|)} E_V$, where g is a dimensionless parameter that scales the perturbational field E_V in relation to an initial field E_0.

First, we apply the disturbance with $g = 0.45$ on the field that is created by bilayer and trilayer structures of a skyrmion bag with $N = 7$ (see Figure 3e). Two exemplary disturbed vector fields are illustrated in Figure 4a and b. A schematic Fourier decomposition is depicted in Figure 4c, where contributions of the initial and disturbance field are colored in purple and orange, respectively. The perturbated field of Figure 4a represents a deformed skyrmion bag with the same topological numbers of the full skyrmion bag S_{bag} and the skyrmion cluster within the bag S_{cluster}. For the derivation of these topological numbers, the integration boundary of the skyrmion number density is set along the black and red dashed lines of Figure 4a which follow the maximum and minimum out-of-plane field components, respectively. The unchanged topology implies that the perturbated field of Figure 4a can be created by a continuous deformation of space from the skyrmion bag of Figure 3e. This is not the case for the perturbated field of Figure 4b which is why this field distribution possesses different topological numbers. Visually the difference can be identified by
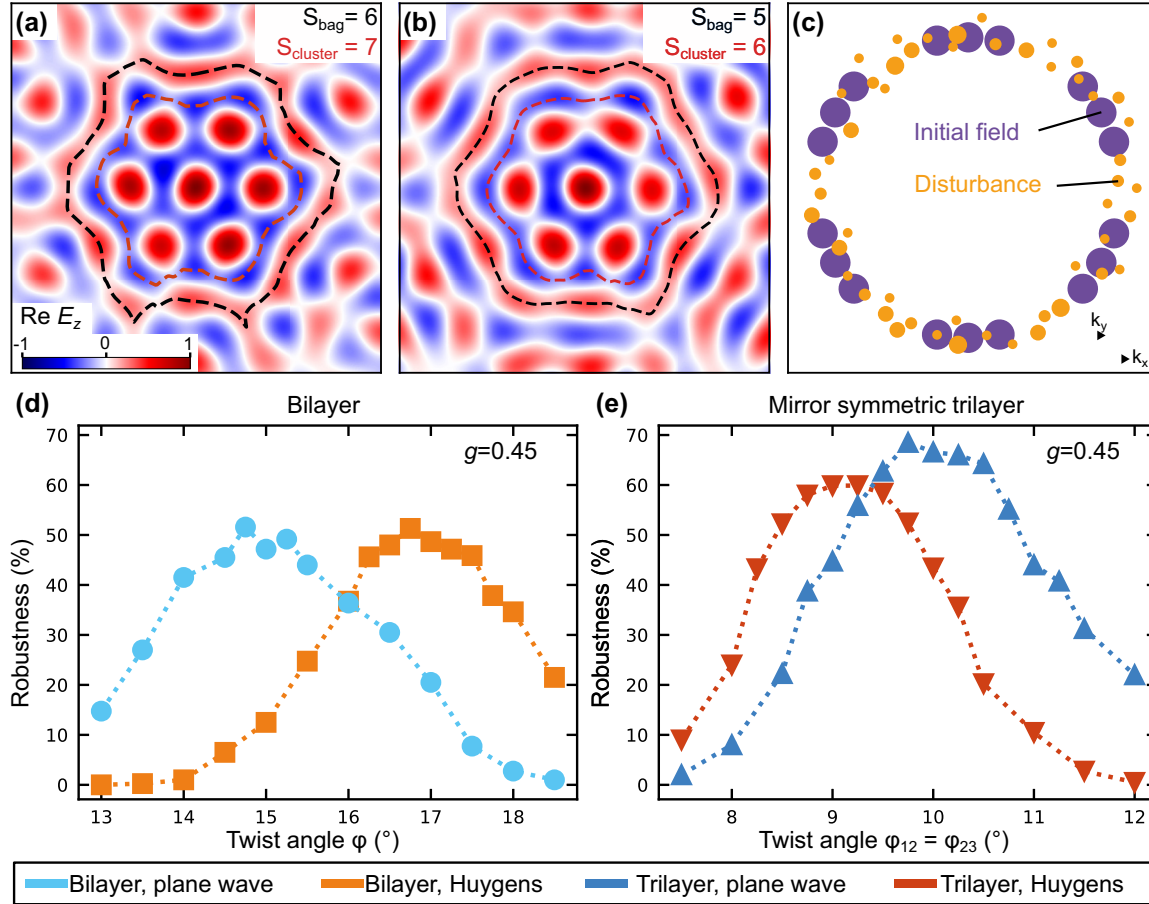
Figure 4: Skyrmion bag robustness. (a, b) Disturbed electric field distribution of the skyrmion bag with $N = 7$ (see Figure 3e). The disturbed field in (a) has the correct (preserved) topology and the disturbed field of (b) has an incorrect (changed) topology. (c) Exemplary Fourier decomposition of the disturbed skyrmion bag. Initial and disturbed field components are colored in purple and yellow, respectively. (d, e) Robustness of the skyrmion bag with $N = 7$ in twisted (d) bilayer and (e) trilayer skyrmion lattices against perturbations in the form of (c). The robustness is defined as the proportion of fields that preserve their topology when the random disturbance is applied. The robustness is presented for initial fields that are calculated using the Huygens approach and in the plane wave approximation.

noticing that two of the cluster skyrmions have merged. This changes the topological numbers to $S_{cluster} = 6$ and $S_{bag} = 5$. Using perturbational fields with other random parameters, the topology might also be changed by skyrmions of the cluster that are connected to the surrounding bag skyrmion, by a splitting of the skyrmions that otherwise overlap to create the bag skyrmion, or by flipped in-plane field components.

With the help of such random disturbance fields, we quantify the robustness of skyrmion bags by the proportion that preserves its topological numbers S_{bag} and $S_{cluster}$ after application of the random perturbation. Using this approach, we can compare the robustness of skyrmion bags in twisted bilayer and mirror symmetric trilayer skyrmion lattices. The robustness is plotted in Figure 4d and e as a function of the twist angles. This analysis is conducted for initial fields that are calculated using two different

methods. In the plane wave approach, the field is calculated using simple interference of SPP plane waves in the limit of infinitely large coupling structures, while in the other case the field is calculated for the exact coupling structure (as in Figure 1b), also considering damping of the SPPs (see Supplementary for details). We note that the comparison between Huygens simulations and plane wave simulations is also important when extending the skyrmion concept from plasmonics to water waves. While the Huygens simulation suits well the plasmonics experiments, the plane wave approximation might be well suited for water waves due to less damping, hence longer propagation lengths and much larger boundary structures from where the waves are emitted.

From the results of Figure 4d and e it can be concluded that the trilayer skyrmion bag of size $N = 7$ is slightly more robust than the bilayer skyrmion bag against field

disturbances that are considered in this approach. In particular, the results show an increase in the robustness from $(52 \pm 1)\%$ to $(60 \pm 1)\%$ for the exact SPP structure and to $(68.5 \pm 1)\%$ for the plane wave interference. The robustness of the exact structure is slightly lower than in the plane wave approach. This is a result of field deviations of the initial field that are attributed to the smaller length of the individual boundaries. In addition to the optimum number of boundaries, we can also derive the ideal twist angles to create the skyrmion bag with optimized robustness which is around 16.75° in the bilayer and 9.25° in the trilayer case.

In the supplementary information we present the resulting robustness of skyrmion bags comprising 1, 2, 4, 10, 12, 14, and 19 skyrmions as a function of their twist angles. From these results we obtain the ideal twist angles of the bilayer and trilayer structures (see Table S1). Using these ideal angles, it is now possible to compare the robustness of the different skyrmion bags.

The results are illustrated in Figure 5 for the plane wave and Huygens wave calculation of the initial field. In general, it is noticed that smaller skyrmion bags of the same rotation center have a higher degree of topological stability that stretches over a larger range of twist
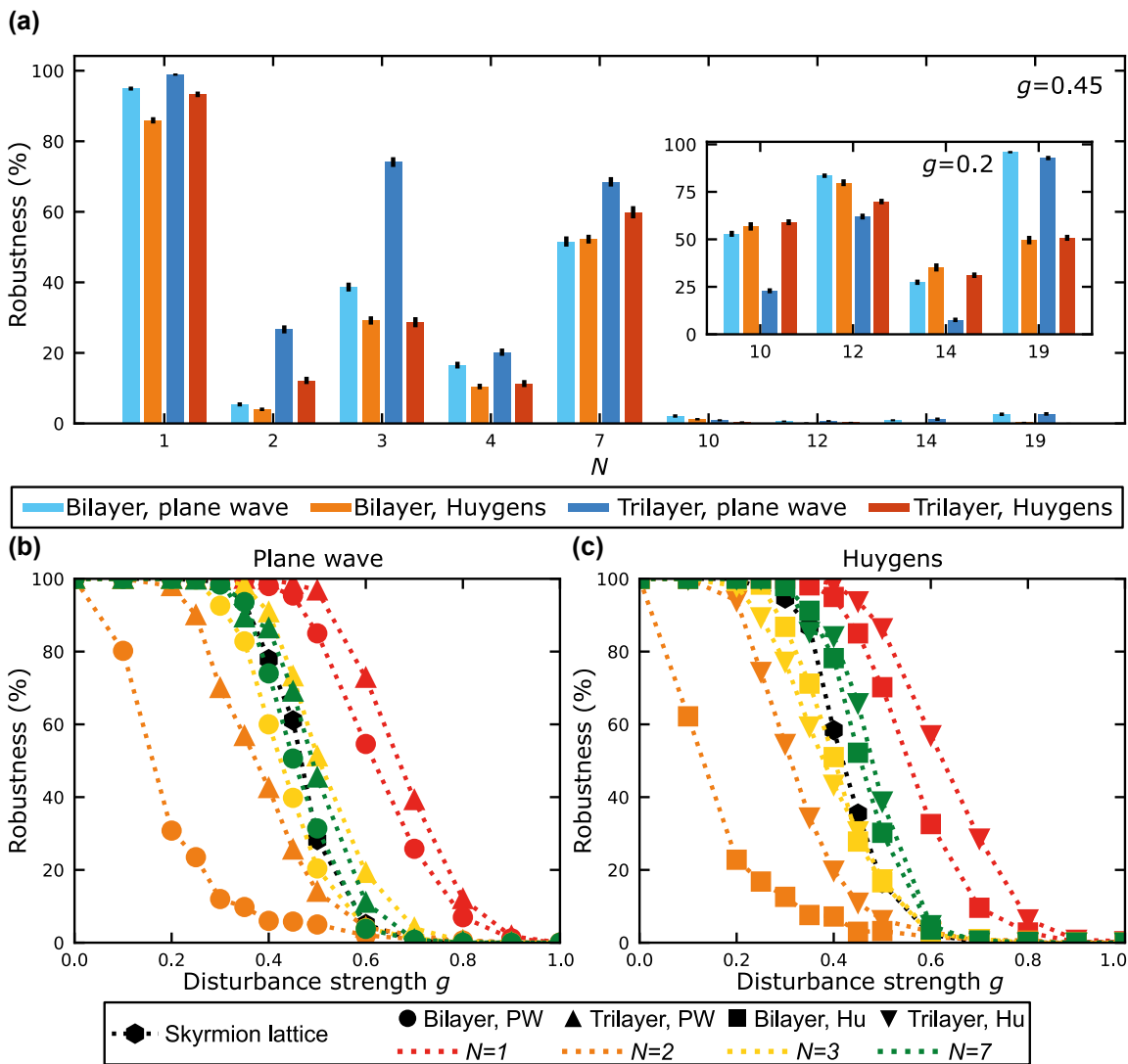

Figure 5: Comparison of skyrmion bag robustness. (a) Comparison of the robustness of all different skyrmion bags of Figure 3. In the inset, the robustness is presented for perturbational fields with lower amplitude to compare the robustness of topologically more unstable skyrmion bags. (b, c) Robustness of skyrmion bags and a skyrmion lattice of seven skyrmions as a function of the disturbance strength g. The results are shown for initial fields that are calculated using the plane wave approximation (b) and the Huygens approach (c). Bilayer and trilayer coupling structures are distinguished by the markers, while the colors correspond to the size of the skyrmion bags.

angles. For different rotation centers, the topological stability varies, which is noticed directly when comparing the robustness of skyrmion bags with $N = 1, 2$, and 3. Additionally, smaller skyrmion bags have a larger robustness for trilayer structures, while bilayer structures show higher robustness for larger skyrmion bags. Using a trilayer structure the displacement of skyrmions is increased, which has two effects. The surrounding bag skyrmion with $S = -1$ becomes more homogeneous, which is beneficial for the topological robustness. However, the cluster skyrmions become more elongated, which leads to a more likely overlap of the cluster skyrmions, especially for large skyrmion bags. In total this leads to trilayer structures being superior for small skyrmion bags and inferior for large skyrmion bags.

In Figure 5b and c the robustness of skyrmion bags with $N = 1, 2, 3$, and 7 are shown as a function of the disturbance strength g. For weak disturbances, the field textures exhibit a high robustness close to 1, which underlies the stability of the topology in this regime. At a disturbance strength, which is specific to each topological feature and its coupling structure, the robustness starts to decay and reaches vanishing values within $\Delta g \leq 0.3$. Lastly, we also want to compare the robustness of skyrmion bags to the robustness of seven skyrmions in the center of a skyrmion lattice, which is also displayed in Figure 5b and c. For $g = 0.45$ the robustness of the skyrmion lattice is calculated to $(35.5 \pm 1)\%$ for the Huygens simulation and $(51.5 \pm 1)\%$ for the plane wave simulation of the initial fields and is therefore comparable to the robustness of a skyrmion bag with $N = 7$. This shows that our method can not only be used to optimize coupling structures but also enables the comparison of different topological features and can therefore be used to assess their chances of a successful experimental realization.

5 Outlook

Our findings provide valuable insights for the measurement of twisted trilayer superlattices and skyrmion bags formed through the interference of plasmonic-like waves. This extends to systems such as phonon polaritonic surface waves [51], acoustic waves [52], and water wave systems [53], [54]. In these contexts, the theoretical framework can be adapted by replacing the surface plasmon polariton waves of the initial and perturbed fields with the corresponding wave types specific to these systems.

In magnetism, skyrmions are formed by electron spin, resulting in topological stability associated with an energy barrier determined by spin interactions. In contrast, skyrmions in optics, plasmonics, and other surface wave systems are not protected by such energy barriers in the absence of light–matter interactions that preserve topological invariants. This distinction has fueled the ongoing debate about the robustness of skyrmions in these systems [32], [35], [55], [56]. Nevertheless, topology in these systems is not without benefit and holds promise for applications in structured light–matter interactions, high-resolution optical microscopy and metrology, and quantum technologies. A deeper understanding of topology-induced robustness against perturbations is therefore essential for advancing these applications. Our analysis represents a foundational approach to quantitatively study and compare the robustness of topological textures. The method is simple, versatile, and extendable to other systems where topological features also arise from wave interference.

Author contributions: HG conceived the idea of trilayer moiré skyrmion superlattices. JS, FM, BF, and HG conceived the idea of commensurability. JS and TJD conceived the idea of testing the topological robustness. JS carried out the simulations, analytical calculations, and skyrmion number analysis with the help of TJD. JS wrote the manuscript and all authors contributed to discussions and final editing. All authors have accepted responsibility for the entire content of this manuscript and approved its submission.
Conflict of interest: Authors state no conflict of interest.
Data availability: The datasets generated and/or analysed during the current study are available from the corresponding author upon reasonable request.

References

[1] Y. Cao, *et al*., "Unconventional superconductivity in magic-angle graphene superlattices," *Nature*, vol. 556, no. 7699, pp. 43−50, 2018.

[2] Y. Cao, *et al*., "Correlated insulator behaviour at half-filling in magic-angle graphene superlattices," *Nature*, vol. 556, no. 7699, pp. 80−84, 2018.

[3] Y. Cao, *et al*., "Strange metal in magic-angle graphene with near planckian dissipation," *Phys. Rev. Lett.*, vol. 124, no. 7, p. 076801, 2020.

[4] J. M. Park, Y. Cao, K. Watanabe, T. Taniguchi, and P. Jarillo-Herrero, "Tunable strongly coupled superconductivity in magic-angle twisted trilayer graphene," *Nature*, vol. 590, no. 7845, 2021, https://doi.org/10.1038/s41586-021-03192-0.

[5] H. Meng, Z. Zhan, and S. Yuan, "Commensurate and incommensurate double moiré interference in twisted trilayer graphene," *Phys. Rev. B*, vol. 107, no. 3, p. 035109, 2023.

[6] Z. Hao, *et al*., "Electric field−tunable superconductivity in alternating-twist magic-angle trilayer graphene," *Science*, vol. 371, no. 6534, pp. 1133−1138, 2021.

[7] Z. Zhu, S. Carr, D. Massatt, M. Luskin, and E. Kaxiras, "Twisted trilayer graphene: a precisely tunable platform for correlated electrons," *Phys. Rev. Lett.*, vol. 125, no. 11, p. 116404, 2020.

[8] H. Kim, *et al*., "Evidence for unconventional superconductivity in twisted trilayer graphene," *Nature*, vol. 606, no. 7914, pp. 494−500, 2022.

[9] A. Uri, *et al*., "Superconductivity and strong interactions in a tunable moiré quasicrystal," *Nature*, vol. 620, no. 7975, pp. 762−767, 2023.

[10] P. Zeller, X. Ma, S. Günther, N. Leconte, and J. Jung, "Commensurate and incommensurate double moire interference in graphene encapsulated by hexagonal boron nitride," *2d Mater.*, vol. 7, no. 3, p. 031005, 2020.

[11] A. Mishchenko, *et al*., "Twist-controlled resonant tunnelling in graphene/boron nitride/graphene heterostructures," *Nat. Nanotechnol.*, vol. 9, no. 10, pp. 808−813, 2014.

[12] G. Chen, *et al*., "Tunable correlated Chern insulator and ferromagnetism in a moiré superlattice," *Nature*, vol. 579, no. 7797, pp. 56−61, 2020.

[13] Z. Lian, *et al*., "Quadrupolar excitons and hybridized interlayer Mott insulator in a trilayer moiré superlattice," *Nat. Commun.*, vol. 14, no. 1, pp. 1−7, 2023.

[14] C. G. Péterfalvi, A. David, P. Rakyta, G. Burkard, and A. Kormányos, "Quantum interference tuning of spin-orbit coupling in twisted van der Waals trilayers," *Phys. Rev. Res.*, vol. 4, no. 2, p. L022049, 2022.

[15] S. Xie, *et al*., "Strong interlayer interactions in bilayer and trilayer moire superlattices," *Sci. Adv.*, vol. 8, no. 12, p. 1911, 2022.

[16] G. Chen, *et al*., "Evidence of a gate-tunable Mott insulator in a trilayer graphene moiré superlattice," *Nature*, vol. 15, no. 3, pp. 237−241, 2019.

[17] J. Chen, X. Lin, M. Chen, T. Low, H. Chen, and S. Dai, "A perspective of twisted photonic structures," *Appl. Phys. Lett.*, vol. 119, no. 24, 2021, https://doi.org/10.1063/5.0070163.

[18] A. González-Tudela and J. I. Cirac, "Cold atoms in twisted-bilayer optical potentials," *Phys. Rev. A*, vol. 100, no. 5, p. 053604, 2019.

[19] P. Wang, *et al*., "Two-dimensional Thouless pumping of light in photonic moiré lattices," *Nat. Commun.*, vol. 13, no. 1, pp. 1−8, 2022.

[20] C. Huang, F. Ye, X. Chen, Y. V. Kartashov, V. V. Konotop, and L. Torner, "Localization-delocalization wavepacket transition in pythagorean aperiodic potentials," *Sci. Rep.*, vol. 6, no. 1, p. 32546, 2016.

[21] Z. Meng, *et al*., "Atomic Bose−Einstein condensate in twisted-bilayer optical lattices," *Nature*, vol. 615, no. 7951, pp. 231−236, 2023.

[22] P. Wang, *et al*., "Localization and delocalization of light in photonic moiré lattices," *Nature*, vol. 577, no. 7788, pp. 42−46, 2019.

[23] Y. V. Kartashov, F. Ye, V. V. Konotop, and L. Torner, "Multifrequency solitons in commensurate-incommensurate photonic moiré lattices," *Phys. Rev. Lett.*, vol. 127, no. 16, p. 163902, 2021.

[24] J. Guan, J. Hu, Y. Wang, M. J. H. Tan, G. C. Schatz, and T. W. Odom, "Far-field coupling between moiré photonic lattices," *Nat. Nanotechnol.*, vol. 18, no. 5, pp. 514−520, 2023.

[25] T. H. R. Skyrme, "A unified field theory of mesons and baryons," *Nucl. Phys.*, vol. 31, pp. 556−569, 1962.

[26] X. Z. Yu, *et al*., "Real-space observation of a two-dimensional skyrmion crystal," *Nature*, vol. 465, no. 7300, pp. 901−904, 2010.

[27] S. Mühlbauer, *et al*., "Skyrmion lattice in a chiral magnet," *Science*, vol. 323, no. 5916, pp. 915−919, 2009.

[28] J. Tang, *et al*., "Magnetic skyrmion bundles and their current-driven dynamics," *Nat. Nanotechnol.*, vol. 16, no. 10, pp. 1086−1091, 2021.

[29] S. Das, *et al*., "Observation of room-temperature polar skyrmions," *Nature*, vol. 568, no. 7752, pp. 368−372, 2019.

[30] J. I. Fukuda and S. Žumer, "Quasi-two-dimensional skyrmion lattices in a chiral nematic liquid crystal," *Nat. Commun.*, vol. 2, no. 1, pp. 1−5, 2011.

[31] D. Foster, C. Kind, P. J. Ackerman, J. S. B. Tai, M. R. Dennis, and I. I. Smalyukh, "Two-dimensional skyrmion bags in liquid crystals and ferromagnets," *Nat. Phys.*, vol. 15, no. 7, pp. 655−659, 2019.

[32] Y. Shen, Q. Zhang, P. Shi, L. Du, X. Yuan, and A. V. Zayats, "Optical skyrmions and other topological quasiparticles of light," *Nat. Photonics*, vol. 18, no. 1, pp. 15−25, 2023.

[33] S. Gao, F. C. Speirits, F. Castellucci, S. Franke-Arnold, S. M. Barnett, and J. B. Götte, "Paraxial skyrmionic beams," *Phys. Rev. A*, vol. 102, no. 5, p. 053513, 2020.

[34] Y. Shen, Y. Hou, N. Papasimakis, and N. I. Zheludev, "Supertoroidal light pulses as electromagnetic skyrmions propagating in free space," *Nat. Commun.*, vol. 12, no. 1, pp. 1−9, 2021.

[35] P. Ornelas, I. Nape, R. de Mello Koch, and A. Forbes, "Non-local skyrmions as topologically resilient quantum entangled states of light," *Nat. Photonics*, vol. 18, no. 3, pp. 258−266, 2024.

[36] S. Tsesses, E. Ostrovsky, K. Cohen, B. Gjonaj, N. H. Lindner, and G. Bartal, "Optical skyrmion lattice in evanescent electromagnetic fields," *Science*, vol. 361, no. 6406, pp. 993−996, 2018.

[37] L. Du, A. Yang, A. V. Zayats, and X. Yuan, "Deep-subwavelength features of photonic skyrmions in a confined electromagnetic field with orbital angular momentum," *Nat. Phys.*, vol. 15, no. 7, pp. 650−654, 2019.

[38] T. J. Davis, D. Janoschka, P. Dreher, B. Frank, F. J. Meyer zu Heringdorf, and H. Giessen, "Ultrafast vector imaging of plasmonic skyrmion dynamics with deep subwavelength resolution," *Science*, vol. 368, no. 6489, p. eaba6415, 2020.

[39] J. Schwab, *et al*., "Plasmonic twistronics: discovery of plasmonic skyrmion bags," arXiv:2411.03032, 2024.

[40] L. Yang, *et al*., "Embedded skyrmion bags in thin films of chiral magnets," *Adv. Mater.*, vol. 36, p. 2403274, 2024.

[41] T. J. Davis, B. Frank, D. Podbiel, P. Kahl, F. J. Meyer Zu Heringdorf, and H. Giessen, "Subfemtosecond and nanometer plasmon dynamics with photoelectron microscopy: theory and efficient simulations," *ACS Photonics*, vol. 4, no. 10, pp. 2461−2469, 2017.

[42] X. Lei, *et al*., "Photonic spin lattices: symmetry constraints for skyrmion and meron topologies," *Phys. Rev. Lett.*, vol. 127, no. 23, p. 237403, 2021.

[43] G. Spektor, *et al*., "Revealing the subfemtosecond dynamics of orbital angular momentum in nanoplasmonic vortices," *Science*, vol. 355, no. 6330, pp. 1187−1191, 2017.

[44] Y. Dai, *et al*., "Ultrafast microscopy of a twisted plasmonic spin skyrmion," *Appl. Phys. Rev.*, vol. 9, no. 1, p. 11420, 2022.

[45] S. Tsesses, K. Cohen, E. Ostrovsky, B. Gjonaj, and G. Bartal, "Spin-orbit interaction of light in plasmonic lattices," *Nano Lett.*, vol. 19, no. 6, pp. 4010−4016, 2019.

[46] R. Lifshitz, "Quasicrystals: a matter of definition," *Found. Phys.*, vol. 33, no. 12, pp. 1703−1711, 2003.

[47] J. M. B. L. dos Santos, N. M. R. Peres, and A. H. C. Neto, "Continuum model of the twisted graphene bilayer," *Phys. Rev. B*, vol. 86, no. 15, p. 155449, 2012.

[48] J. M. Campanera, G. Savini, I. Suarez-Martinez, and M. I. Heggie, "Density functional calculations on the intricacies of moiré patterns on graphite," *Phys. Rev. B Condens. Matter Mater. Phys.*, vol. 75, no. 23, p. 235449, 2007.

[49] X. Zhao, *et al*., "Commensurate and incommensurate double moire interference in graphene encapsulated by hexagonal boron nitride," *2d Mater.*, vol. 7, no. 3, p. 031005, 2020.

[50] J. D. Correa, M. Pacheco, and E. S. Morell, "Optical absorption spectrum of rotated trilayer graphene," *J. Mater. Sci.*, vol. 49, no. 2, pp. 642−647, 2014.

[51] F. Mangold and E. Bau, "Discovery of phonon-polaritonic skyrmions: transition from bubble- to Néel-type," In preparation.

[52] H. Ge, *et al*., "Observation of acoustic skyrmions," *Phys. Rev. Lett.*, vol. 127, no. 14, p. 144502, 2021.

[53] D. A. Smirnova, F. Nori, and K. Y. Bliokh, "Water-wave vortices and skyrmions," *Phys. Rev. Lett.*, vol. 132, no. 5, p. 054003, 2024.

[54] B. Wang, *et al*., "Topological water-wave structures manipulating particles," *arXiv:2406.08515*, 2024. https://doi.org/10.48550/arXiv .2406.08515.

[55] C. Liu, S. Zhang, S. A. Maier, and H. Ren, "Disorder-induced topological state transition in the optical skyrmion family," *Phys. Rev. Lett.*, vol. 129, no. 26, 2022, https://doi.org/10.1103/ PHYSREVLETT.129.267401.

[56] I. Nape, *et al*., "Revealing the invariance of vectorial structured light in complex media," *Nat. Photonics*, vol. 16, no. 7, pp. 538−546, 2022.